# In Situ Fabrication of Inorganic Nanowire Arrays Grown from and Aligned on Metal Substrates

WEIXIN ZHANG[*,†] AND SHIHE YANG[*,‡]

[†]School of Chemical Engineering, Hefei University of Technology, Hefei, Anhui 230009, P. R. China, [‡]Department of Chemistry, William Mong Institute of Nano Science and Technology, The Hong Kong University of Science and Technology, Clear Water Bay, Kowloon, Hong Kong, P. R. China

CONSPECTUS
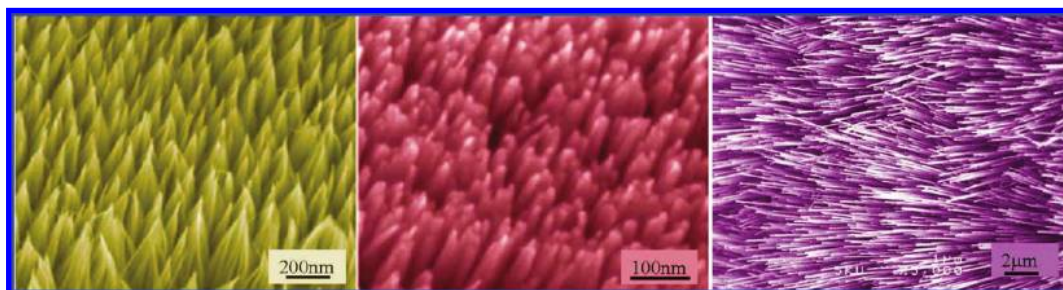
The full potential of nanotechnology can be unleashed only when one is able not only to synthesize a rich variety of nano-scale building blocks but also assemble them into various patterns at the supramolecular and supracluster levels. In particular, the application of nanoparticle and nanowire materials often requires their assembly in the form of thin films, preferably on conductive surfaces for electrical addressing, control, and detection. Although a dazzling array of nanostructures has been fabricated by bottom-up approaches, one of the contemporary challenges is to assemble these nanostructures so that they introduce and realize functionalities. An alluring avenue is to simultaneously accomplish both the nanostructure synthesis and assembly on a useful substrate in a parallel fashion, affording the advantages of simplicity, low cost, and high throughput.

In this Account, we review our recent work on growing inorganic nanowires (for example, metal sulfides, metal oxides, and so forth) directly from and on metal substrates in arrays without using templates and catalysts. This method of engineering nano-wire arrays on metal substrates integrates the nanowire synthesis and assembly into a parallel process, both in time and in space, by exploiting in situ chemistry on the metal substrates. Both gas-phase and solution-phase approaches have been developed to synthesize the aligned nanowires; here, full advantage is taken of interfacial kinetics of restricted diffusion and surface-specific reactions, often accompanied by new interfacial growth mechanisms. The setting of nanowire arrays on metal substrates has allowed exploration of their application potentials in areas such as field electron emission and chemical sensing.

The approaches described here are general, and we predict that they will be extended to more inorganic materials, such as metal halides. Moreover, as more control is achieved with synthetic methods, inorganic nanowire arrays should provide unusual magnetic, optical, and electronic properties for nanostructural engineers willing to confront the attendant challenges. Accordingly, applications for which there is a current impetus for progress, such as solar cells or lithium ion secondary batteries, might well be addressed with this methodology.

Introduction

The last two decades have witnessed an explosive development in the bottom-up synthesis of nanostructured materials, ranging from fullerenes and carbon nanotubes to nanoparticles and nanowires.[1−5] Harnessing these novel nanomaterials for device applications, however, necessitates their assembly into ordered nanostructured arrays or higher level nanoarchitectures. The assembled nanostructures are expected to not only have an enhanced collective response to external stimuli, for example, electromagnetic fields or chemical

species, but also build synergetic multifunctionalities into an integral system of a device.

Nanowires distinguish themselves from other nanomaterials by their unique one-dimensionality (1D), which is anticipated to be important for fundamental research and future nanotechnology.[6,7] For example, 1D systems exhibit peculiar electronic structures including density of states singularities, molecule-like states over large distances, and spin-charge separation associated with a Luttinger liquid. Practically, nanowires could become crucial elements for new nanoscale devices owing to their unique properties. After all, 1D is the smallest dimension for efficient transport of electrons and optical excitations, which at least qualifies nanowires as interconnections for nanoscale devices.

The anisotropy of nanowires renders them more difficult to assemble than spherical nanoparticles into a large structure of any dimensionality, be it a horizontal or a vertical array. Whereas postassembly strategy has been used to obtain horizontal nanowire arrays via solvent flow through microfluidic channels[8] and by the Langmuir−Blodgett deposition,[9,10] it is difficult to apply to vertical nanowires arrays. Yet vertical nanowire arrays display many desirable characteristics for device integrations, such as enhanced capacity and rate capability in lithium ion batteries[11,12] and improved light coupling and electron lifetime in dye-sensitized solar cells.[13]

Traditionally, vertical nanowire arrays were fabricated by the use of templates such as membranes of anodic aluminum oxide (AAO) and track-etched polycarbonate. Ozin et al.[14] and Martin et al.[15] first used nanoporous membranes as templates to prepare arrays of nanotubes and nanorods. Although the template method is general and flexible, the removal of template turned out to be a hassle and often accompanied by aggregation. Vertical nanowire arrays can also be fabricated by vapor−liquid−solid (VLS)[16,17] and oxide-assisted[18] processes. However, the VLS approach and its analogues generally require catalysts, high temperature, or both, which may limit some of their applications.

For the past few years, our research group has been working on an alternative strategy to integrate the growth and assembly of nanowires on metal substrates. The defining characteristic of our strategy is that the metal substrate itself is part of the reactants to sustain the nanowire growth into a vertical array without using templates and catalysts. The parallel synthesis and assembly of nanowire arrays obviate the need for postassembly and have the advantages of simplicity, mild reaction conditions, and low cost, opening up a promising avenue for engineering nanodevices. This Account summarizes our work on the in situ fabrication and assembly of nanowire
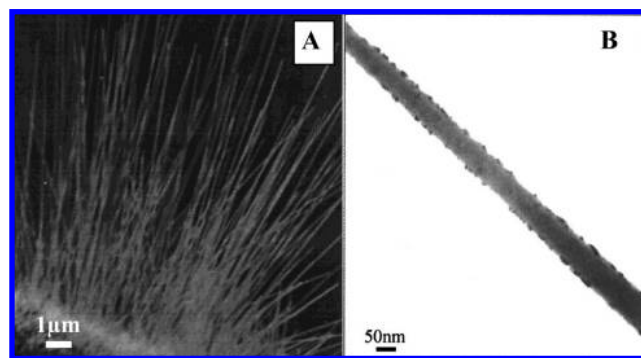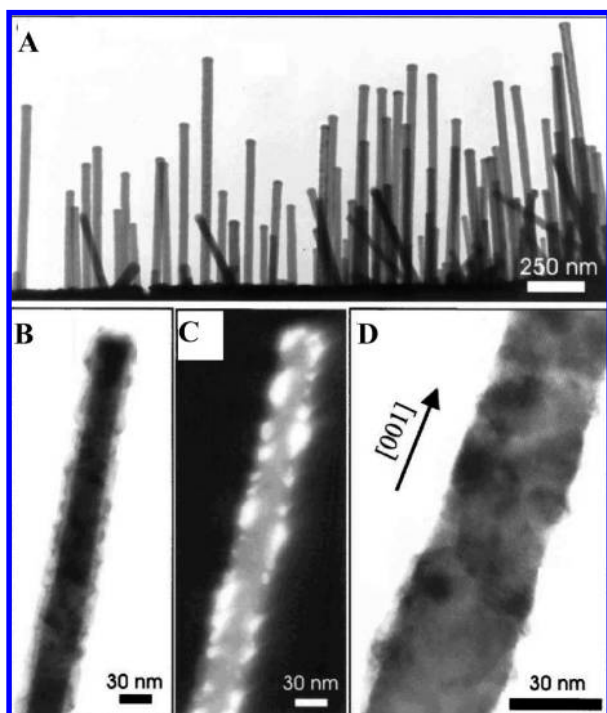

FIGURE 1. (A) SEM image of a Cu_2S nanowire array grown on a copper foil. (B) TEM image of a single Cu_2S nanowire.

arrays on metal substrates. In the following, we present some selected results in four sections on gas−solid synthesis, solution−solid synthesis, core/sheath fabrication, and properties and potential applications of the nanowire arrays. Finally, we will conclude and give the future prospects of this research area.

Gas−Solid Reaction Approach to the Synthesis of Inorganic Nanowire Arrays

Metal Sulfide Nanowire Arrays. Copper sulfide was the first system with which we succeeded in growing nanowire arrays on a copper substrate by the gas−solid (GS) approach.[19,20] The reaction conditions were unusually simple and mild: by exposing a well-cleaned copper foil into an atmosphere of O_2 and H_2S at room temperature, we obtained a black film homogeneously covering the copper substrate, which turned out to be a uniform array of Cu_2S nanowires. The array consists of straight Cu_2S nanowires (Figure 1A) with a diameter of $\sim50-70$ nm and length of $\sim7-16$ μm, which are aligned approximately perpendicular to the substrate surface. These nanowires are crystalline, and some of them have a thin layer of oxide coating (fcc Cu_2O) at the surface (Figure 1B) due to the presence of reactive O_2.

In order to understand the intriguing nanowire growth mechanism, we examined early stages of the Cu_2S nanowire development.[21] When the reaction time between the copper surface and the gas mixture of H_2S/O_2 was 10 min, mainly a Cu_2O layer was observed. Cu_2S nuclei started to appear on the Cu_2O layer for reaction time >20 min. After nucleation, the Cu_2S nanostructures then evolved into nanowires and grew mainly along the direction perpendicular to the copper surface (~100 min). A more extended growth period resulted in well-aligned Cu_2S nanowires as shown in Figure 2A. The nanowires are not only straight but also uniform in diameter ($d = \sim40$ nm) and have lengths of a few hundred nanometers. It seems that there is an induction period for the nucle-

FIGURE 2. (A) TEM image of Cu_2S nanowires grown on the surface of a TEM copper grid. (B−D) core/shell structure, dark-field image using $(200)_{Cu_2S}$ diffraction (bright dot contrast comes from the Cu_2O shell), and HRTEM image of a Cu_2S nanowire. Reproduced from ref 21. Copyright 2009 Elsevier.

ation of incipient Cu_2S nanowires, after which the 1D growth is much faster. Interestingly, each nanowire consists of an inner single-crystalline core and an outer shell as can be seen more clearly in Figure 2B. By combination of the selected area electron diffraction (SAED) and dark-field imaging, it was verified that the inner core of single-crystalline Cu_2S is enclosed by an outer shell of polycrystalline Cu_2O (Figures 2C,D).

We found that O_2 is essential to the formation of the Cu_2S nanowires on a copper surface despite the reaction $Cu(s) + H_2S(g) = Cu_2S(s) + H_2(g)$ being exergonic at room temperature ($\Delta G° = -52.8$ KJ/mol). The nanowire formation is believed to start with an oxidation reaction $2Cu(s) + 1/2O_2(g) = Cu_2O(s)$, followed by sulfidation $Cu_2O(s) + H_2S(g) = Cu_2S (s) + H_2O(g)$. These processes probably correspond to the induction period for the nanowire nucleation mentioned above. The well-established VLS growth mechanism is not supported by our experiments; we never observed a drop-like feature at the nanowire tips. Nevertheless, the nanowire assembly site has to be at one of the two ends, the root or the tip. The root-growth mechanism might be at work because the close-by copper surface can provide the necessary feeding materials for the nanowire growth. In this mechanism, however, the assembly process would be kinetically hindered at this site. More important, the root-growth mechanism cannot explain why the

Cu_2S nanowires thicken or thin as the reaction proceeds. On the other hand, the tip-growth mechanism appears to explain all the facts observed so far. Here the growth is on the nanowire tip and the feeding stocks are from the roots. This demands a reasonably efficient transport channel for the feeding stocks, e.g., copper ions, across or through the nanowires.

The nanowire growth mechanism is summarized in Figure 3. After the nucleation of Cu_2S from sulfidation of Cu_2O (panels A−C), Cu_2S proceeds with 1D growth vertically (panels C,D) driven by its crystalline anisotropy. To sustain the nanowire growth, O_2 is adsorbed on the nanowire tip and reduced, leaving electron holes and Cu^+ vacancies on the nanowire tip. Both the electron holes and the Cu^+ vacancies migrate through the Cu_2S nanowire from the tip down to the root and are annihilated there. The Cu_2O species thus formed on the nanowire tip is then converted to Cu_2S by the reaction with H_2S. The nanowire assembly continues in this way on the tip by interweaving the sulfur and copper layers in alternation. A similar mechanism was proposed for the growth of Cu_2S thin films on copper surfaces.[22] Most recently, CuTCNQ nanowire arrays were also found to grow in this way.[23]

The GS approach was also successfully used to prepare Ag_2S nanowires on silver substrates.[24] When a preoxidized silver substrate was exposed to an atmosphere of an O_2/H_2S mixture at room temperature or slightly above, Ag_2S nanowires were abundantly produced with diameters of 40−150 nm and aspect ratios up to ~1000. Our results suggest that the diameter and morphology of the nanowires are mainly controlled by the nanowire growth rate and the diffusion rate of Ag^+ ions from the substrate to the nanowire active site. At low temperatures, Ag^+ diffusion in the growing nanowire is expected to be slow. As the nanowire grew longer and longer, the Ag^+ supply became shorter and shorter to sustain the uniform nanowire growth, resulting in the formation of a nanocone structure with a sharp tip. As the temperature was increased, however, the atomic diffusion rate of Ag increased, which provided a sufficient amount of Ag^+ at the nanowire tip for the growth. Consequently, the individual nanowire diameters were more uniform with relatively blunt tips. This strongly supports the tip-growth mechanism of the Ag_2S nanowires.

Metal Oxide Nanowire Arrays. One of the problems with the GS growth of metal oxide nanowire arrays is that metal ion diffusion is commonly slower in the metal oxides than in the corresponding sulfides. Increasing the reaction temperature, use of appropriate oxidative gases, and judicious choice of metal/metal oxide systems could be viable solutions.
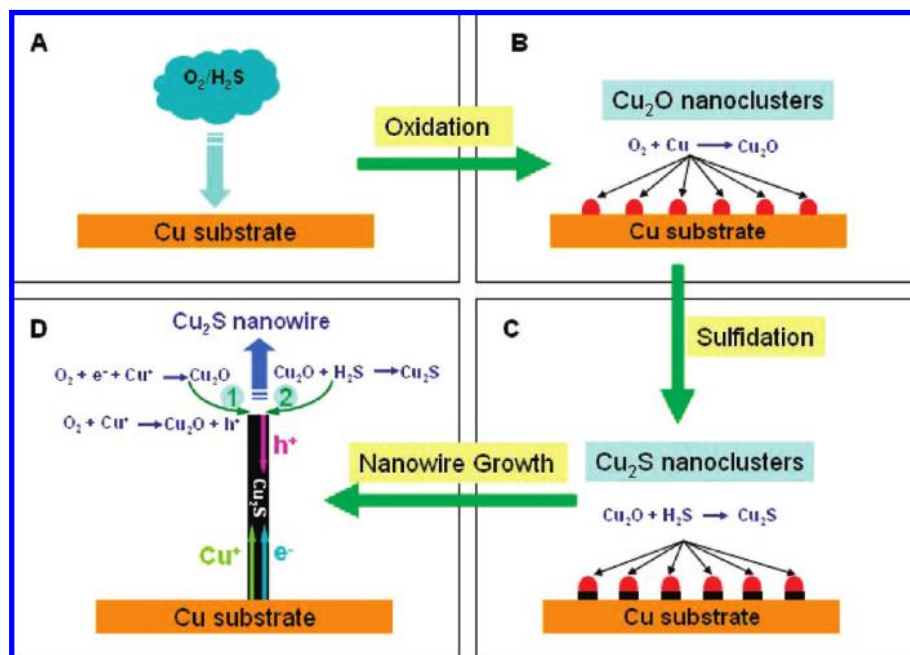
FIGURE 3. Schematic tip-growth mechanism of Cu_2S nanowire arrays on copper surface: (A) Cu surface in the presence of O_2 and H_2S; (B) formation of Cu_2O nanoclusters; (C) formation of Cu_2S nanoclusters; (D) tip growth of Cu_2S nanowires.
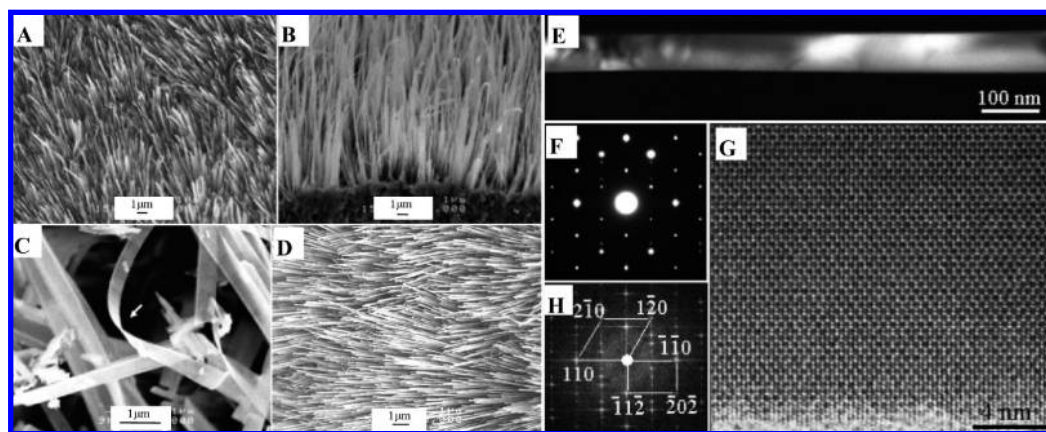
**FIGURE 4.** α-Fe_2O_3 nanobelt and nanowire arrays on iron substrates: (A,B) Top view and side view SEM images of a nanobelt array grown at 700 °C; (C) high-magnification SEM image of the nanobelts transferred from the substrate; (D) bird's eye view SEM image of a nanowire array synthesized at 800 °C; (E−H) dark-field TEM image, SAED pattern, and HRTEM (FFT) image of an α-Fe_2O_3 nanowire.

Indeed, ZnO nanobelt arrays[25] and α-Fe_2O_3 nanobelt/nanowire arrays[26] have been successfully synthesized from and on zinc and iron substrates, respectively, by the GS reaction approach at elevated temperatures but still lower than or close to the melting points of the metals.

Direct thermal oxidation under a flow of O_2 produced α-Fe_2O_3 nanobelts in the low-temperature region ($\sim$700 °C), but cylindrical nanowires were formed at relatively higher temperatures ($\sim$800 °C). Both nanobelts and nanowires are mostly bicrystallites with a length of tens of micrometers, which grow uniquely along the [110] direction. The growth habits of the nanobelts and nanowires in the two tempera-

ture regions indicate the role of growth rate anisotropy and surface energy in dictating the ultimate nanomorphologies.

Figure 4A,B shows SEM images for the samples prepared at 700 °C. Clearly, only wire-like features were produced, which are aligned in a dense array approximately perpendicular to the substrate surface with a uniform coverage. Close examination of the products rubbed from the substrate surface revealed that the wire-like features are actually nanobelts with a thickness of several nanometers (Figure 4C). In general, the nanobelts obtained under our growth conditions are about 5−10 nm in thickness, 30−300 nm in width, and 5−50 μm in length.
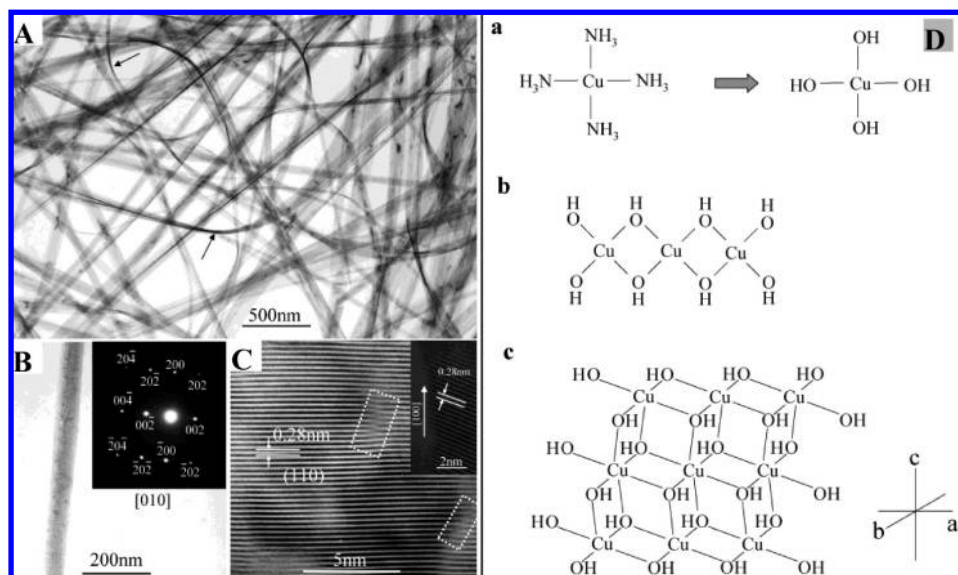
FIGURE 5. (A) TEM image of Cu(OH)$_2$ nanoribbons grown on a copper grid. (B) TEM image and ED pattern (inset) of a single Cu(OH)$_2$ nanoribbon. (C) HRTEM images of a nanoribbon and its boundary section (inset). (D) Schematic illustration of the coordination assembly of the Cu(OH)$_2$ nanoribbons.

Shown in Figure 4D−H are nanowires prepared at 800 °C. The diffraction contrast (E) suggests a cylindrical wire morphology, while the SAED pattern (F) indicates a bicrystal structure, confirmed by the HRTEM image (G) and FFT (H). It is clear that most of the synthesized α-Fe$_2$O$_3$ nanobelts and nanowires have a bicrystal structure, and the nanostructures grow uniquely along the [110] direction.

The peculiar morphologies from the 1D growth of α-Fe$_2$O$_3$ lend further support to the tip-growth mechanism. First, the 1D growth of α-Fe$_2$O$_3$ is along the [110] direction. We suggested that the (110) plane, being O-rich and Fe-deficient, is more reactive, driving more efficient Fe^{3+} transport and thus the belt growth in the [110] direction. Second, narrowing and thinning of the nanobelts occur with the lapse of reaction time due to a short supply of Fe^{3+} ions for long nanobelts. Finally, we found that low-temperature synthesis prefers the formation of nanobelts, and high-temperature synthesis favors the growth of nanowires. This nanobelt-to-nanowire morphology transition, although related to surface energy, is also at least partly caused by different ion diffusion rates along different crystal directions at different temperatures; in particular, accelerated Fe^{3+} diffusion along the wire direction contributes to the formation of nanowires in lieu of the tapered nanobelts.

Solution−Solid Reaction Approach to the Fabrication of Nanowire Arrays

The nature of solution−solid (SS) reaction assembly of inorganic nanowire arrays suggests different mechanisms at work from those of the GS method because here the solvent can be an effective carrier for reactive ion transport. The SS method consists of an initial nucleation at the substrate and the subsequent 1D vertical growth with the supply of metal ions generated from the metal substrate and transported to the nanowire tip.

Copper Hydroxide and Oxide Nanowire Arrays. By using the SS approach with either Cu$_2$S nanowires as sacrificial precursor[27] or bare copper surface under O$_2$,[28] we obtained well-aligned Cu(OH)$_2$ nanoribbon arrays on copper foil in an ammonia alkaline solution. For the bare copper surface under O$_2$, the reactions probably proceed as follows:
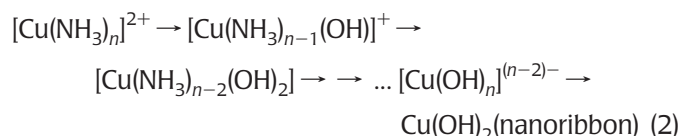
$$Cu + O_2 + NH_3 \rightarrow Cu[NH_3]_n^{2+} \quad (1)$$

$$[Cu(NH_3)_n]^{2+} \rightarrow [Cu(NH_3)_{n-1}(OH)]^+ \rightarrow$$
$$[Cu(NH_3)_{n-2}(OH)_2] \rightarrow \rightarrow \ldots [Cu(OH)_n]^{(n-2)-} \rightarrow$$
$$Cu(OH)_2(\text{nanoribbon}) \quad (2)$$

Figure 5 shows a TEM image of the Cu(OH)$_2$ nanoribbons grown directly from the copper grid at room temperature for 12 h. The thinning in the bend and wring sections, which would not occur for cylindrical nanowires (see arrows in A), demonstrates the ribbon-like morphology. These nanoribbons have widths of 20−130 nm and thicknesses of a few nanometers along the whole lengths of several tens of micrometers. Figure 5B shows a low magnification TEM image of a typical single Cu(OH)$_2$ nanoribbon with a width of 60 nm. Although some tiny cavities can be seen on the surface, the nanoribbon is actually a single crystal, as is evidenced by the corresponding ED pattern (inset of panel B). The spotted selected area ED pattern appears to be associated with the [010] zone axis of orthorhombic Cu(OH)$_2$, and it shows that

the growth direction of a single nanoribbon is [100]. A HRTEM image of the single nanoribbon is shown in Figure 5C. The clear fringes with a spacing of 0.28 nm match well the distance between the (110) crystal planes. As the inset of Figure 5C shows, the [110] direction makes an angle (∼20°) with the axis of the nanoribbon, which is close to the angle between [100] and [110] of orthorhombic $Cu(OH)_2$. This further confirms the nanoribbon growth direction of [100].

The formation of the $Cu(OH)_2$ nanoribbons can be explained by a type of coordination assembly. The idea is schematically shown in Figure 5D. As is well-known, Cu^{2+} prefers square-planar coordination by OH^- (a), and this leads to an extended chain (b), which is actually the final nanoribbon direction. The chains can be juxtaposed together through coordination of the OH^- group to the d_{z^2} orbital of Cu^{2+}, forming a 2D structure (c), which controls the width of the final nanoribbon. Finally, the 2D layers are stacked together through the relatively weak hydrogen bonds and become a 3D crystal. Essentially, the bonding nature in the different crystal directions dictates the growth rates and thus the final nanoribbon morphology.

Through further heat treatment at 120−180 °C with a constant flow of N_2, $Cu(OH)_2$ nanoribbon arrays were transformed to CuO without obvious morphological changes.

$$Cu(OH)_2 \xrightarrow{\Delta} CuO + H_2O \qquad (3)$$
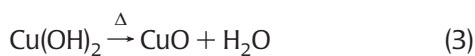
Shown in Figure 6 are SEM and TEM images of $Cu(OH)_2$ and CuO nanoribbon films. The $Cu(OH)_2$ nanoribbons cover the copper surface uniformly, smoothly, and compactly (A) and are roughly aligned perpendicular to the copper surface (B). After heat treatment, CuO nanoribbon arrays were formed. As is shown in Figure 6C, although somewhat shrunken, the ribbon-like morphology is well-preserved. The SAED pattern together with the XRD profile confirms the complete conversion of the $Cu(OH)_2$ nanoribbons to CuO nanoribbons. Shown in Figure 6E is the SEM image of a CuO nanoribbon array obtained after reaction at 5 °C for 96 h. Apparently, the CuO nanoribbons still keep the aligned structure on the Cu substrate. The HRTEM image in Figure 6F shows that the single CuO nanoribbon is a crystal though the crystallinity is not perfect with wavy or discontinuous fringes.

With stronger oxidants and bases, such as $(NH_4)_2S_2O_8$ and NaOH, a series of 1D nanostructured arrays of $Cu(OH)_2$ and CuO were obtained.[29,30] In general, the formation of $Cu(OH)_2$ and CuO nanostructures on copper surface involves complicated reactions of polycondensation and dehydration through competing processes of dissolution−precipitation. The mor-
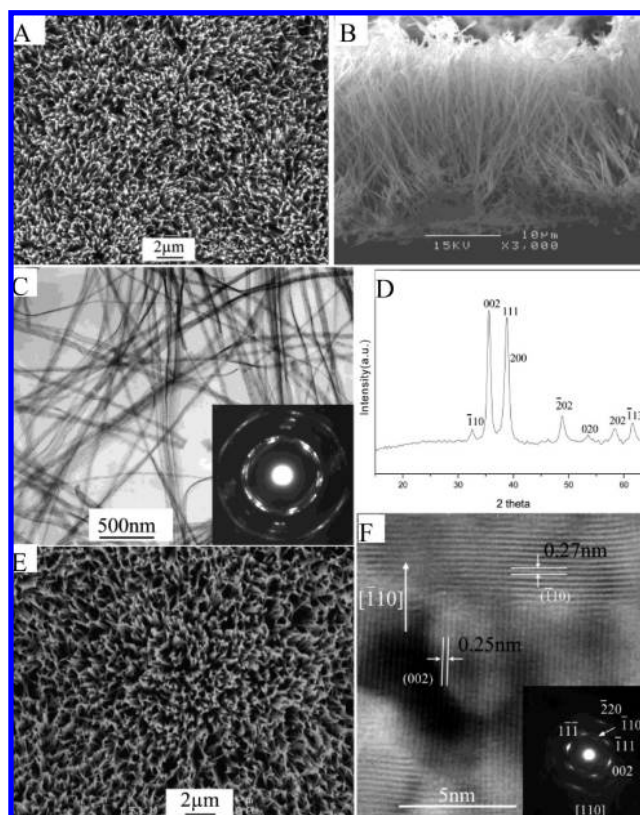

FIGURE 6. (A) Top view and (B) side view SEM images of $Cu(OH)_2$ nanoribbon arrays. (C) TEM image and (D) XRD pattern of CuO nanoribbon arrays transformed from $Cu(OH)_2$. (E) Top view SEM image of the CuO nanoribbon array. (F) HRTEM image and SAED pattern of a single CuO nanoribbon.

phological evolution is highly dependent on the synthetic conditions. Our use of a strong oxidant and base appears to make possible the formation of some intermediate phases such as $Cu(OH)_2$ nanofibers and nanotubes, and CuO nanosheets, nanostrips, and nanobelts.

Ultrathin ZnO 1D Nanostructured Arrays. Hydrothermal treatment of a zinc substrate in an ammonia/alcohol/water mixed solution resulted in ultrathin ZnO nanofibers aligned on the zinc substrate.[31] The ZnO nanofibers are ultrathin (3−10 nm) with a length of ∼500 nm. The growth mechanism of the ultrathin ZnO nanofibers appears to be very similar to that of $Cu(OH)_2$ nanobelts described above. In developing the SS approach, we sought to get more handles on the control over nanowire growth on the substrate by applying electrical potentials. With the electrochemical deposition method, both ultrathin ZnO nanobelts and ZnO nanorods as thin as 8 nm in ordered arrays on the Zn cathode were synthesized in alkaline solutions of amine−alcohol mixtures.[32,33]
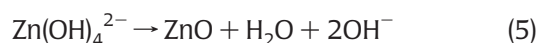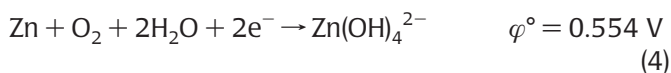
Although ZnO was found to be deposited on both anode and cathode of Zn foils, vertically arrayed ZnO nanorods were
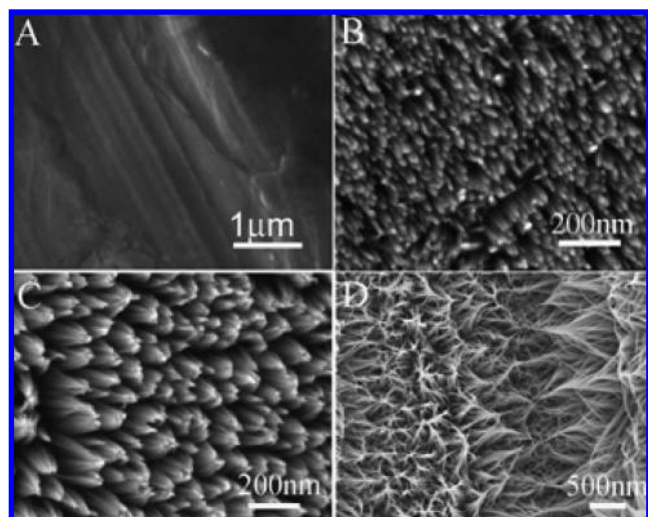
FIGURE 7. SEM images of ZnO products on a Zn cathode at various applied electric potentials: (A) 0; (B) 0.4; (C) 1.5; (D) 3.8 V. Other conditions: $[H_2O_2]$ = 22 mM; pH = 12.

only produced on the cathode. Our results showed that the cathode can nucleate ZnO through oxidation of Zn by electrolysis-generated O_2. The growth of ZnO nanorods is sustained either by electrochemical oxidation of the anode or by chemical oxidation of the cathode. Figure 7 shows the effect of applied electric potentials. No 1D nanostructure of ZnO can be found in the absence of the applied electric potential (A). When an electric potential of 0.4 V was applied, vertically arrayed ZnO nanorods were produced on the cathode (B). Further increase of the potential to 1.5 V resulted in the formation of the slightly longer ZnO nanobelts (200 nm), which were assembled roughly into a bundle-like morphology (C). When the potential was finally elevated to 3.8 V, ZnO nanobelts as long as 1 μm were obtained, and they were assembled completely into dense nanobundles to minimize surface energy (D).

The 1D arrays of ZnO are thought to form by the following cathode reactions in conjunction with in situ nucleation and the subsequent 1D tip growth:

$$Zn + O_2 + 2H_2O + 2e^- \rightarrow Zn(OH)_4^{2-} \qquad \varphi^\circ = 0.554 \text{ V} \tag{4}$$

$$Zn(OH)_4^{2-} \rightarrow ZnO + H_2O + 2OH^- \tag{5}$$

## In Situ Fabrication of Core/Sheath Nanowire Arrays

Surface modification of nanowire arrays with a conducting nanolayer is expected to add more functionalities and may even lead to completely new nanocomposite materials, which may be useful in sensors, detectors, rechargeable batteries, and energy and information processing devices.
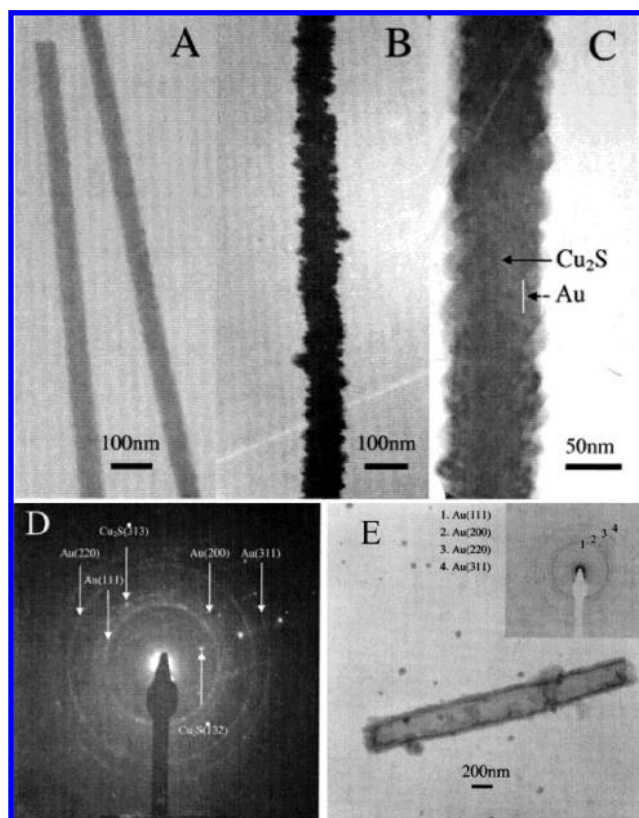
FIGURE 8. TEM images of Cu_2S nanowires before (A) and after (B, C) Au coating. (D) ED pattern of a single Cu_2S/Au core/sheath nanowire. (E) TEM image and ED pattern of a gold nanotube after removal of the Cu_2S core from a Cu_2S/Au core/sheath nanowire.

Cu_2S/Au Core/Sheath Nanowire Arrays. The gold-coating on the Cu_2S nanowires was accomplished via the redox reactions of galvanic cells.[34] During the redox processes, the Cu_2S nanowires act as cathodes where Au deposition occurs, and the copper substrate serves as an anode where copper dissolution takes place. The electrolyte was the coating solution containing $HAuCl_4$. At least during the initial phase, the Cu_2S nanowires as a fairly good electric conductor short the circuits, ensuring the continuation of the gold-coating reactions. Later on, the gold sheath itself should constitute a much better conducting path. Because the reduction potential of $AuCl_4^-$/Au is much higher than that of Cu^{2+}/Cu, the deposition of Au on the Cu_2S nanowires and the simultaneous dissolution of Cu from the copper substrate were spontaneous.

Typical TEM images of the Cu_2S nanowires are shown in Figure 8 before (A) and after the gold coating (B, C). Before coating, the nanowires are ~60 nm in diameter and have a relatively smooth surface (A). On immersion of the nanowires in a coating solution for 1 h, the diameter of the nanowire was increased to ~100 nm (B, C). Although the nanowire surface became rougher after coating, it appears to be compactly covered by the gold deposit along the entire length of
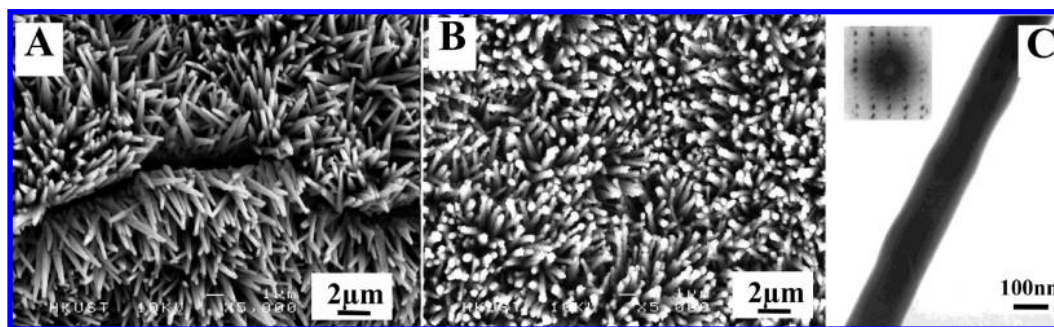
FIGURE 9. SEM images of a bare Cu_2S nanowire array (A) and a PPY-coated Cu_2S nanowire array (B) obtained with a pyrrole polymerization time of 2.0 h. (C) TEM image and SAED pattern a single PPY-coated Cu_2S nanowire.

the nanowire. The roughness of the nanowire surface indicates that the gold coating is polycrystalline probably because Au was deposited on the Cu_2S nanowire surfaces in the form of Au nanocrystals aggregated to form a continuous coating layer. The ED pattern in Figure 8D confirms the polycrystalline nature of the outer sheath of Au (ring pattern) as well as the single-crystal nature of the inner core of Cu_2S (discrete diffraction spots).

For the Cu_2S/Au core/sheath nanowires, the core of Cu_2S could be removed by etching with acid to form gold nanotubes. Figure 8E shows the TEM picture of such a gold nanotube obtained after immersion in an acidic solution for an extended period of time. It has a diameter of ~300 nm and a wall thickness of 50 nm. Clearly, one end of the gold tube is closed and the other is open. The ED pattern (inset) shows the polycrystalline fcc structure of the gold tube and the absence of diffraction features from Cu_2S originally residing in the core.

Cu_2S/Polypyrrole Core/Sheath Nanowire Arrays. Polypyrrole (PPY) as a typical conducting polymer (CP) offers reasonably high conductivity and good environmental stability. However, the inherent intractability of PPY has prevented it from being blended with other materials to form nanocomposites using conventional techniques. Although nanoparticles of inorganic core and CP shell were synthesized by coating[35] and catalytic in situ polymerization,[36] the CP often precipitated and could not be easily separated from the core/shell nanoparticles. By using an interfacial polymerization technique, we succeeded in coating Cu_2S nanowires with a homogeneous and well-adhered layer of PPY 20−50 nm thick.[37] The PPY coating could be controlled at the interfacial layer of chloroform and water by polymerization time, PY concentration, and PY-to-oxidant ratio.

The PPY-coating result is shown in Figure 9. The arrayed Cu_2S nanowires used for PPY coating are ~5 μm long, isolated from each other, and roughly perpendicular to the substrate surface (A). After in situ pyrrole polymerization for 2 h,

the nanowire morphology is clearly preserved (B). In addition, no PPY precipitate can be seen in the gaps between the PPY-coated Cu_2S nanowires, indicating that the thin PPY layers are closely attached to the Cu_2S cores. The TEM image in Figure 9C displays a core/shell nanowire after pyrrole polymerization. One can see that the Cu_2S nanowire core with a diameter of 65 nm is closely encapsulated by a conformal coating layer of PPY 20 nm thick. The SAED in the inset of Figure 9C proves that the single-crystalline structure of the inner core of Cu_2S remained unchanged. We believe that the PPY layer shall improve not only the conductivity but also the stability and mechanical properties of the Cu_2S nanowires, which are otherwise environmentally sensitive and mechanically brittle.

Properties and Potential Applications of the Nanowire Arrays

The unique setting of nanowires aligned on a conducting substrate have facilitated the studies on properties and applications of these novel materials in field emission,[38,39] gas sensors,[25] dye-sensitized solar cells/photoelectrochemical devices,[40] field effect transistors,[41] etc. In the following, we select some preliminary results to exemplify our efforts in this direction.

Field Electron Emission. Although carbon nanotubes (CNTs) are an excellent field emission material, the field emission properties depend on whether the CNTs are metallic or semiconducting. Unfortunately, one is still unable to control these properties using the presently available synthetic methodologies. Our nanowire arrays may be a good alternative for field emission devices because the materials are semiconductors and could be grown on metal substrates by an incredibly simple method.

The field emission uniformity from nanowire arrays and its variation with field were examined using the transparent anode technique. Figure 10A presents a plot of the emission current vs field ($I-E$) for a Cu_2S nanowire device.[38] Field emission was observed at ~6 MV/m, and a typical threshold field
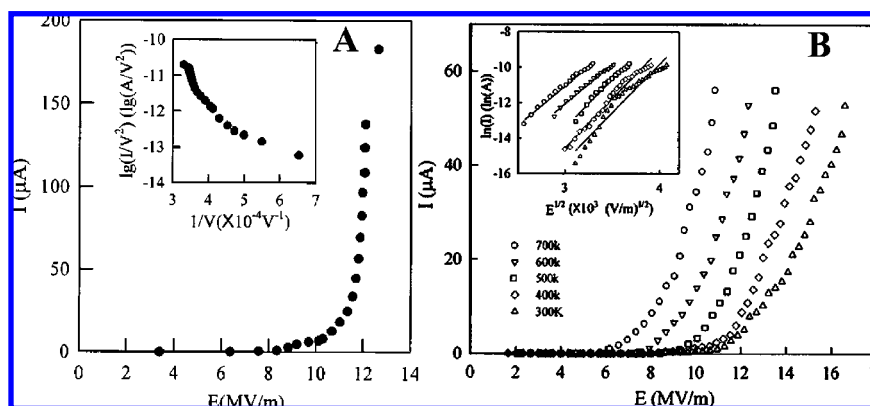
**FIGURE 10.** (A) *I−E* curve of a Cu$_2$S nanowire array film. Inset is the corresponding FN plot. (B) *I−E* curve of CuO nanobelt array films measured at different temperatures. The inset shows the corresponding ln(I)−$E^{1/2}$ plots. Reproduced from refs 38 and 39. Copyright 2009 American Institute of Physics.

for obtaining a current density of 1 μA/mm^2 is 11 MV/m. The corresponding Fowler−Nordheim plot in the inset of Figure 10A exhibits nonlinearity, which could be explained by the diverse field enhancement factor of the nanowires. Specifically, the Cu$_2$S nanowires have different radii and lengths, and therefore the field enhancements for different nanowires are varied, which would result in different turn-on fields for the individual nanowires. This conforms to the emission site imaging result; that is, more emission sites are turned on at higher fields.

Field-emission characteristics of aligned CuO nanobelts were also studied using the transparent anode technique.[39] By heating the substrate, reproducible emission currents were recorded at different temperatures in the range of 300−750 K. Figure 10B shows typical *I−E* plots at 300−700 K. No obvious decay of the emission current was observed during ∼30 h of operation in this temperature range. SEM postinspection of the nanobelt films showed no change in morphology. From the plots shown in Figure 10B, it can be derived that the threshold field for obtaining a current density of 10 mA/cm^2 is ∼11 MV/m at room temperature and 6 MV/m at 700 K. At a fixed field of 10 MV/m, we observed about 3 orders of magnitude increase of the emission current. This demonstrates that the CuO nanobelt array is a promising cathode material for field emission based thermoelectric devices.

Gas Sensitivity. Here we use ZnO nanobelt arrays with a top electrode to illustrate gas sensor applications.[25] ZnO was extensively used as an NH$_3$-sensing material but mostly in the form of a thin film at high temperature, and no prior measurements of ZnO nanowire sensor responses to NH$_3$ were reported. Our ZnO nanobelt sensor consisted of a low-resistance Si as one of the electrodes and an ITO slide as another electrode pressed on the ZnO nanobelt array. To improve the contact between the ZnO nanobelt array and the ITO elec-
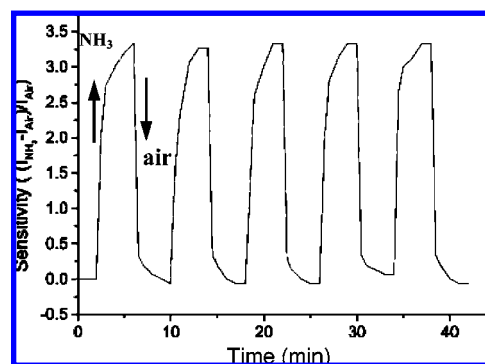
FIGURE 11. Current responses of a ZnO nanobelt array film sensor when the surrounding gas is switched between air and 500 ppm NH$_3$.

trode, a thin soft indium film was formed on the ITO. Figure 11 shows the current response of the sensor to NH$_3$ at room temperature at a bias voltage of 5 V. When exposed to 500 ppm NH$_3$, a current change as high as about 3.5-fold between the on and off states was observed, and this current response to NH$_3$ could be repeated many times without obvious change in sensitivity. The time for the current response to reach 80% of its highest value is about 2 min after adding NH$_3$ and that for it to reach 80% of its lowest value is about 30 s after removing NH$_3$. Apparently, the ZnO nanobelt arrays grown from Zn substrate show both high sensitivity and reversibility at room temperature. For NH$_3$ sensors with ZnO, the current response is mainly caused by the adsorption/desorption of NH$_3$ and H$_2$O molecules on the surface of the sensing material. Therefore the high surface-to-volume ratio of our ZnO nanobelts sensor with the uniformly exposed (0001) surface gives rise to high sensitivity to NH$_3$. Moreover, whereas conventional thin-film sensors require an elevated temperature to facilitate molecular desorption, our nanobelt array sensor has available interbelt spaces for the adsorbed molecules

to desorb easily in the off state so that it shows a rapid response and good reversibility.

Conclusions and Perspectives

We have reviewed our efforts on reactive assembly of aligned inorganic nanowires on metal substrates by GS and SS chemical approaches, which allowed large ordered arrays of metal sulfides and oxides to be prepared directly on metal substrates without using templates and catalysts. This kind of chemical approach to nanostructural engineering features process simplicity, mildness, and scalability, and holds potential for controlling the nucleation/growth, and thus the composition, crystal structure, size, and morphology of the nanostructured arrays by using the established arsenal of chemical knowledge. We also demonstrated that the as-prepared nanowire arrays can be surface-functionalized by an ultrathin layer of metal, conducting polymer, etc. Devices fabricated from these ordered nanowire arrays on metal substrates have displayed outstanding optical, field emission, and gas-sensing properties.

We foresee that the approaches described here will be extended to more inorganic material systems such as metal halides. Moreover, the recent rapid development in nanoelectronics will facilitate the application of aligned nanowire arrays that have been available due to the development of the synthetic methods. Looking ahead, while further advancement in the synthetic methodology for inorganic nanowire arrays with better control is expected, characterizations of the electrical, magnetic, optical, and electronic properties of the nanowire arrays appear to be desirable, challenging, and fruitful endeavors. This will certainly give a great impetus to applications of the inorganic nanowire arrays such as in solar cells and lithium ion secondary batteries.

BIOGRAPHICAL INFORMATION

Weixin Zhang studied chemistry in Hefei University of Technology and received a B.S. in 1990 and a M.S. in 1993. She received her Ph.D. in Inorganic Chemistry in 2000 from the University of Science and Technology of China. From 2001 to 2002, she worked as a visiting scholar in Prof. Shihe Yang's group at the Hong Kong University of Science and Technology. She has been a faculty member in Hefei University of Technology since 1993 and became a full professor in 2000. Her research interests include controlled synthesis of ordered nanostructured arrays and advanced inorganic functional materials and exploration of their potential applications in energy conversion, environmental protection, and micro/nanodevices.

Shihe Yang received his B.S. (1982) in Chemistry from Sun Yat-Sen University in China. Through the US-China CGP program, he was admitted to Rice University in 1983 and obtained a Ph.D. in Physical Chemistry in 1988 (with Prof. Richard E. Smalley). He did postdoctoral research at Argonne National Laboratory and the University of Toronto (with Prof. John C. Polanyi) before joining the faculty at The Hong Kong University of Science and Technology in 1992, where he is currently a full professor. He has been active in understanding the structure, dynamics, and photochemistry of isolated clusters and complexes in the gas phase. Currently, his research interests range from fundamental understanding and manipulation to more down to earth technological applications of zero-, one-, and two-dimensional nanosystems.

FOOTNOTES

*E-mail addresses: wxzhang@hfut.edu.cn; chsyang@ust.hk.

REFERENCES

1 Kratschmer, W.; Lamb, L. D.; Fostiropoulos, K.; Huffman, D. R. Solid C_{60}: A New Form of Carbon. *Nature* **1990**, *347*, 354–358.

2 Iijima, S. Helical Microtubules of Graphitic Carbon. *Nature* **1991**, *354*, 56–58.

3 Alivisatos, A. P. Perspectives on the Physical Chemistry of Semiconductor Nanocrystals. *J. Phys. Chem.* **1996**, *100*, 13226–13239.

4 Hu, J. T.; Odom, T. W.; Lieber, C. M. Chemistry and Physics in One Dimension: Synthesis and Properties of Nanowires and Nanotubes. *Acc. Chem. Res.* **1999**, *32*, 435–445.

5 Pan, Z. W.; Dai, Z. R.; Wang, Z. L. Nanobelts of Semiconducting Oxides. *Science* **2001**, *291*, 1947–1949.

6 Huang, Y.; Duan, X. F.; Cui, Y.; Lauhon, L. J.; Kim, K. H.; Lieber, C. M. Logic Gates and Computation from Assembled Nanowire Building Blocks. *Science* **2001**, *294*, 1313–1317.

7 Wang, Z. L.; Song, J. H. Piezoelectric Nanogenerators Based on Zinc Oxide Nanowire Arrays. *Science* **2006**, *312*, 242–246.

8 Lee, S. H.; Lee, H. J.; Oh, D.; Lee, S. W.; Goto, H.; Buckmaster, R.; Yasukawa, T.; Matsue, T.; Hong, S. K.; Ko, Cho, M. W.; Yao, T. Control of the ZnO Nanowires Nucleation Site Using Microfluidic Channels. *J. Phys. Chem. B* **2006**, *110*, 3856–3859.

9 Whang, D.; Jin, S.; Lieber, C. M. Nanolithography Using Hierarchically Assembled Nanowire Masks. *Nano Lett.* **2003**, *3*, 951–954.

10 Acharya, S.; Panda, A. B.; Belman, N.; Efrima, S.; Golan, Y. A Semiconductor-Nanowire Assembly of Ultrahigh Junction Density by the Langmuir-Blodgett Technique. *Adv. Mater.* **2006**, *18*, 210–213.

11 Kim, J. H.; Khanal, S.; Islam, M.; Khatri, A.; Choi, D. Electrochemical Characterization of Vertical Arrays of Tin Nanowires Grown on Silicon Substrates as Anode Materials for Lithium Rechargeable Microbatteries. *Electrochem. Commun.* **2008**, *10*, 1688–1690.

12 Li, Y. G.; Tan, B.; Wu, Y. Y. Mesoporous Co_3O_4 Nanowire Arrays for Lithium Ion Batteries with High Capacity and Rate Capability. *Nano Lett.* **2008**, *8*, 265–270.

13 Wang, H. W.; Ting, C. F.; Hung, M. K.; Chiou, C. H.; Liu, Y. L.; Liu, Z. W.; Ratinac, K. R.; Ringer, S. P. Three-Dimensional Electrodes for Dye-Sensitized Solar Cells: Synthesis of Indium-Tin-Oxide Nanowire Arrays and ITO/TiO_2 Core-Shell Nanowire Arrays by Electrophoretic Deposition. *Nanotechnology* **2009**, *20*, 1–9.

14 Ozin, G. A. Nanochemistry: Synthesis in Diminishing Dimensions. *Adv. Mater.* **1992**, *4*, 612–649.

15 Martin, C. R. Nanomaterials: A Membrane-Based Synthetic Approach. *Science* **1994**, *266*, 1961–1966.

16 Wang, X. D.; Song, J. H.; Li, P.; Ryou, J. H.; Dupuis, R. D.; Summers, C. J.; Wang, Z. L. Growth of Uniformly Aligned ZnO Nanowire Heterojunction Arrays on GaN, AlN, and $Al_{0.5}Ga_{0.5}N$ Substrates. *J. Am. Chem. Soc.* **2005**, *127*, 7920–7923.

17 He, R. R.; Gao, D.; Fan, R.; Hochbaum, A. I.; Carraro, C.; Maboudian, R.; Yang, P. D. Si Nanowire Bridges in Microtrenches: Integration of Growth into Device Fabrication. *Adv. Mater.* **2005**, *17*, 2098–2102.

18 Yao, Y.; Li, F. H.; Lee, S. T. Oriented Silicon Nanowires on Silicon Substrates from Oxide-Assisted Growth and Gold Catalysts. *Chem. Phys. Lett.* **2005**, *406*, 381–385.

19 Wang, S. H.; Yang, S. H. Surfactant-Assisted Growth of Crystalline Copper Sulphide Nanowire Arrays. *Chem. Phys. Lett.* **2000**, *322*, 567–571.

20 Wang, S. H.; Yang, S. H. Growth of Crystalline Cu_2S Nanowire Arrays on Copper Surface: Effect of Copper Surface Structure, Reagent Gas Composition, and Reaction Temperature. *Chem. Mater.* **2001**, *13*, 4794–4799.

21 Wang, N; Fung, K. K.; Wang, S.; Yang, S. Oxide-Assisted Nucleation and Growth of Copper Sulphide Nanowire Arrays. *J. Cryst. Growth* **2001**, *233*, 226–232.

22 Larson, R. S. A Physical and Mathematical Model for the Atmospheric Sulfidation of Copper by Hydrogen Sulfide. *J. Electrochem. Soc.* **2002**, *149*, B40−B46.

23 Ji, H. X.; Hu, J. S; Guo, Y. G.; Song, W. G.; Wan, L. J. Ion-Transfer-Based Growth: A Mechanism for CuTCNQ Nanowire Formation. *Adv. Mater.* **2008**, *20*, 4879–4882.

24 Wen, X. G.; Wang, S. H.; Xie, Y. T.; Li, X. Y.; Yang, S. H. Low Temperature Synthesis of Single Crystalline Ag_2S Nanowires on Silver Substrates. *J. Phys. Chem. B* **2005**, *109*, 10100–10106.

25 Wen, X. G.; Fang, Y. P.; Pang, Q.; Yang, C. L.; Wang, J. N.; Ge, W. K.; Wong, K. S.; Yang, S. H. ZnO Nanobelt Arrays Grown Directly from and on Zinc Substrates: Synthesis, Characterization, and Applications. *J. Phys. Chem. B* **2005**, *109*, 15303–15308.

26 (a) Wen, X. G.; Wang, S. H.; Ding, Y.; Wang, Z. L.; Yang, S. H. Controlled Growth of Large-Area, Uniform, Vertically Aligned Arrays of α-Fe_2O_3 Nanobelts and Nanowires. *J. Phys. Chem. B* **2005**, *109*, 215–220. (b) Fu, Y. Y.; Wang, R. M.; Xu, J.; Chen, J.; Yan, Y.; Narlikar, A. V.; Zhang, H. Synthesis of Large Arrays of Aligned α-Fe_2O_3 Nanowires. *Chem. Phys. Lett.* **2003**, *379*, 373–379.

27 Wen, X. G.; Zhang, W. X.; Yang, S. H.; Dai, Z. R.; Wang, Z. L. Solution Phase Synthesis of $Cu(OH)_2$ Nanoribbons by Coordination Self-Assembly Using Cu_2S Nanowires as Precursors. *Nano Lett.* **2002**, *2*, 1397–1401.

28 Wen, X. G.; Zhang, W. X.; Yang, S. H. Synthesis of $Cu(OH)_2$ and CuO Nanoribbon Arrays on Copper Surface. *Langmuir* **2003**, *19*, 5898–5903.

29 Zhang, W. X.; Wen, X. G.; Yang, S. H.; Berta, Y.; Wang, Z. L. Single Crystalline Scroll-Type Nanotube arrays of Copper Hydroxide Synthesized at Room Temperature. *Adv. Mater.* **2003**, *15*, 822–825.

30 Zhang, W. X.; Wen, X. G.; Yang, S. H. Controlled Reactions on a Copper Surface: Synthesis and Characterization of Nanostructured Copper Compound Films. *Inorg. Chem.* **2003**, *42*, 5005–5014.

31 Fang, Y. P.; Pang, Q.; Wen, X. G.; Wang, J. N.; Yang, S. H. Synthesis of Ultrathin ZnO Nanofibres Aligned on a Zn Substrate. *Small* **2006**, *2*, 612–615.

32 Yang, J. H.; Qiu, Y. F.; Yang, S. H. Studies of Electrochemical Synthesis of Ultrathin ZnO Nanorod/Nanobelt Arrays on Zn Substrates in Alkaline Solutions of Amine-Alcohol Mixtures. *Cryst. Growth Des.* **2007**, *7*, 2562–2567.

33 Yang, J. H.; Liu, G. M.; Lu, J.; Qiu, Y. F.; Yang, S. H. Electrochemical Route to the Synthesis of Ultrathin ZnO Nanorods/Nanobelts Arrays on Zinc Substrate. *Appl. Phys. Lett.* **2007**, *90*, 103109.

34 Wen, X. G.; Yang, S. H. Cu_2S/Au Core/Sheath Nanowires Prepared by A Simple Redox Deposition Method. *Nano Lett.* **2002**, *2*, 451–454.

35 McCarthy, G. P.; Armes, S. P.; Greaves, S. J.; Watts, J. F. Synthesis and Characterization of Carboxylic Acid Functionalized Polypyrrole Silica Microparticles Using a 3-Substituted Pyrrole Comonomer. *Langmuir* **1997**, *13*, 3686−3692.

36 Huang, C. L.; Matijevic, E. Coating of Uniform Inorganic Particles with Polymers. 3. Polypyrrole on Different Metal-Oxides. *J. Mater. Res.* **1995**, *10*, 1327–1336.

37 Zhang, W. X.; Wen, X. G.; Yang, S. H. Synthesis and Characterization of Uniform Arrays of Copper Sulfide Nanorods Coated with Nanolayers of Polypyrrole. *Langmuir* **2003**, *19*, 4420–4426.

38 Chen, J.; Deng, S. Z.; Xu, N. S.; Wang, S. H.; Wen, X. G.; Yang, S. H.; Yang, C. L.; Wang, J. N.; Ge, W. K. Field Emission from Crystalline Copper Sulphide Nanowire Arrays. *Appl. Phys. Lett.* **2002**, *80*, 3620–3622.

39 Chen, J.; Deng, S. Z.; Xu, N. S.; Zhang, W. X.; Wen, X. G.; Yang, S. H. Temperature-Dependence of Field Emission from Cupric Oxide-Nanobelt Films. *Appl. Phys. Lett.* **2003**, *83*, 746–748.

40 (a) Anandan, S.; Wen, X. G.; Yang, S. H. Room Temperature Growth of CuO Nanorod Arrays on Copper and Their Application as a Cathode in Dye-Sensitized Solar Cells. *Mater. Chem. Phys.* **2005**, *93*, 35–40. (b) Yang, S. F.; Wen, X. G.; Zhang, W. X.; Yang, S. H. Photoelectrochemistry of Pure and Core/Sheath Nanowire Arrays of Cu_2S Directly Grown on Copper Electrodes. *J. Electrochem. Soc.* **2005**, *152*, 220–226.

41 Fan, Z. Y.; Wen, X. G.; Yang, S. H.; Lu, J. G. Controlled *p*- and *n*- Type Doping of Fe_2O_3 Nanobelt Field Effect Transistors. *Appl. Phys. Lett.* **2005**, *87*, 013113.